Research article

Floating solar panels on reservoirs impact phytoplankton populations: A modelling experiment

Giles Exley [a,*], Trevor Page [a], Stephen J. Thackeray [b], Andrew M. Folkard [a], Raoul-Marie Couture [c], Rebecca R. Hernandez [d,e], Alexander E. Cagle [d,e], Kateri R. Salk [f], Lucie Clous [g], Peet Whittaker [g], Michael Chipps [h], Alona Armstrong [a,i]

[a] *Lancaster Environment Centre, Library Avenue, Lancaster University, Lancaster, LA1 4YQ, United Kingdom*
[b] *Lake Ecosystems Group, UK Centre for Ecology & Hydrology, Lancaster Environment Centre, Bailrigg, Lancaster, LA1 4AP, United Kingdom*
[c] *Department of Chemistry and Center for Northern Studies (CEN), Takuvik Joint International Laboratory, Université Laval, Quebec, Canada*
[d] *Department of Land, Air and Water Resources, UC Davis, Davis, CA, USA*
[e] *Wild Energy Initiative, John Muir Institute of the Environment, UC Davis, California, USA*
[f] *Tetra Tech, Research Triangle Park, NC, USA*
[g] *JBA Consulting, 1 Broughton Park, Skipton, BD23 3FD, United Kingdom*
[h] *Thames Water Research, Development and Innovation, Kempton Park AWTW, Feltham Hill Road, Hanworth, TW13 6XH, United Kingdom*
[i] *Energy Lancaster, Science & Technology Building, Lancaster University, Lancaster, LA1 4YF, United Kingdom*

ARTICLE INFO

ABSTRACT

Floating solar photovoltaic (FPV) deployments are increasing globally as the switch to renewable energy intensifies, representing a considerable water surface transformation. FPV installations can potentially impact aquatic ecosystem function, either positively or negatively. However, these impacts are poorly resolved given the challenges of collecting empirical data for field or modelling experiments. In particular, there is limited evidence on the response of phytoplankton to changes in water body thermal dynamics and light climate with FPV. Given the importance of understanding phytoplankton biomass and species composition for managing ecosystem services, we use an uncertainty estimation approach to simulate the effect of FPV coverage and array siting location on a UK reservoir. FPV coverage was modified in 10% increments from a baseline with 0% coverage to 100% coverage for three different FPV array siting locations based on reservoir circulation patterns. Results showed that FPV coverage significantly impacted thermal properties, resulting in highly variable impacts on phytoplankton biomass and species composition. The impacts on phytoplankton were often dependent on array siting location as well as surface coverage. Changes to phytoplankton species composition were offset by the decrease in phytoplankton biomass associated with increasing FPV coverage. We identified that similar phytoplankton biomass reductions could be achieved with less FPV coverage by deploying the FPV array on the water body's faster-flowing area than the central or slower flowing areas. The difference in response dependent on siting location could be used to tailor phytoplankton management in water bodies. Simulation of water body-FPV interactions efficiently using an uncertainty approach is an essential tool to rapidly develop understanding and ultimately inform FPV developers and water body managers looking to minimise negative impacts and maximise co-benefits.

1. Introduction

Falling costs and the drive to decarbonise global energy supplies have led to widespread uptake of renewable energy sources, including solar photovoltaic (PV) technology. Solar PV has traditionally been dominated by ground- and rooftop-mounted installations. However, since 2007, water-deployed floating solar photovoltaics (FPV) have emerged as an alternative, especially in land-scarce areas (Cagle et al.,

2020). FPV deployment has been rapid, with over 2.6 GW of installed capacity globally (Haugwitz, 2020) and an anticipated annual growth rate of 28.9% between 2020 and 2027. Estimates show that there is technical potential for FPV to produce almost 10% of current national generation in the United States (Spencer et al., 2019), based on a water surface coverage of 27% on suitable water bodies. At a continental scale, FPV covering less than 1% of the surface of African hydropower dams could equal the generation from existing hydropower dams, the largest source of renewable energy across the continent (Sanchez et al., 2021).

FPV is comprised of PV modules attached to a series of floats moored on the surface of a water body (Sahu et al., 2016). Host water bodies tend to be artificial (e.g. raw water reservoirs) and may be used for drinking water provision, irrigation or hydroelectric power generation (Momayez et al., 2009; Lee et al., 2020; Exley et al.,– 2021b). Deploying PV panels on water delivers enhanced performance and electricity generation over ground-based PV due to the cooling effect of the hosting water body (Choi et al., 2013; Sacramento et al., 2015; Yadav et al., 2016; Oliveira-Pinto and Stokkermans, 2020) and reduces land use and land-cover change for renewable energy (Cagle et al., 2020). FPV is deployed at a range of coverages, that is, the percentage of the water surface transformed to host FPV relative to the water body area. Coverage depends on the size of the host water body, the FPV design and the rated capacity of the installation (Exley et al., 2021a).

FPV represents an unprecedented change in the use of artificial water bodies. Understanding impacts is critical as water bodies provide numerous essential ecosystem goods and services, including water for consumption, water quality regulation, and supporting biodiversity (Maltby et al., 2011; Reynaud and Lanzanova, 2017; Grizzetti et al., 2019). Impacts on the host water body could be significant, as light intensity and wind shear will be modified by the shading and sheltering effect of an FPV installation (Armstrong et al., 2020; Haas et al., 2020). Consequently, there is a pressing need to understand and predict the effects of FPV on water body processes and functions (Lee et al., 2020; Stiubiener et al., 2020; Zhang et al., 2020; Gorjian et al., 2021; Ziar et al., 2021). In particular, understanding changes to phytoplankton is critical, given their role as primary producers in aquatic ecosystems (Reynolds, 2006), the increased likelihood of harmful algal blooms under climate change (Ho et al., 2019), and the subsequent implications for recreation and potable water supply (Chapra et al., 2017). Moreover, surface cover proxies for FPV (e.g. ice) suggest that deployments could alter physicochemical habitat conditions in a way that would affect phytoplankton biomass and species composition (Wright, 1964; Danilov and Ekelund, 2001; Lenard and Wojciechowska, 2013; Yamamichi et al., 2018; Exley et al., 2021b).

Given the limited understanding of water body response to FPV deployment, investigations that rapidly develop knowledge should be prioritised. *In-situ* monitoring studies have quantified the impact of FPV installations on water temperatures (de Lima et al., 2021) and aquatic plants (Ziar et al., 2021). However, comprehensive empirical studies are resource-intensive and largely impractical when considering multiple deployment scenarios (Meyer et al., 2009; Janssen et al., 2015). Several studies have hypothesised potential effects of FPV, but these are often conflicting given the complexity of water body functioning. For example, it is claimed that water column shading beneath FPV installations will reduce phytoplankton growth (Armstrong et al., 2020; Lee et al., 2020). Yet, an evidence review of natural and human-made water surface covers found that surface cover may cause a shift to low-light adapted nuisance species, rather than a reduction in total biomass (Yamamichi et al., 2018; Exley et al., 2021b). Numerical modelling 'experiments' provide a less time- and resource-demanding alternative for rapidly testing multiple hypotheses on potential FPV interactions without being limited to a single FPV design, sited on a specific part of a single water body for a limited time. However, given the limited empirical observations so far and limited data to parameterise models, conventional modelling approaches may be unsuitable (Page et al., 2018). Therefore, approaches that can account for the uncertainty associated with sparse input parameters or forcing data are necessary.

Our overarching aim was to determine if FPV coverage and siting location, based on areas of differing circulation, influence phytoplankton biomass and species composition in a reservoir. We used an extended version of the MyLake model with enhanced phytoplankton representation to simulate FPV water quality impacts across discrete zones of a water body. Moreover, we employed an uncertainty estimation approach, a practical solution to overcome the problems associated with limited input data, model parameterisation and validation of simulated output. We also discuss the implications of our findings for water body management and the application of the expanded model for future FPV deployments.

2. Methodology

2.1. MyLake FPV model

To determine if FPV array siting location affects water body thermal properties, phytoplankton biomass and functional-type dynamics, we extended an existing open-source lake model, *MyLake v2* (Markelov et al., 2019). Full details on the original *MyLake* can be found in Saloranta and Andersen (2007) and the accompanying user manual (Saloranta and Andersen, 2004).

2.1.1. MyLake – existing model description

MyLake v2 (Markelov et al., 2019) is a one-dimensional process-based model capable of simulating the daily vertical distributions of water body temperature, phytoplankton, and dissolved and particulate substances, as well as interactions at the sediment-water interface (Saloranta and Andersen, 2007). *MyLake* has been successfully applied to various projects as a standalone simulation tool. For example, assessing ice regime (Livingstone and Adrian, 2009), lake thermodynamics (Woolway et al., 2017), greenhouse gas emissions (Kiuru et al., 2018), light dynamics (Pilla and Couture, 2021) and predicting cyanobacterial blooms (Moe et al., 2016).

Like many one-dimensional lake models (e.g. General Lake Model; Hipsey et al. (2019), General Ocean Turbulence Model; Umlauf et al. (2005), PROTECH; Reynolds et al. (2001)), *MyLake* computes horizontal layer volumes from interpolated water body bathymetric data. In the original version of *MyLake*, the model could simulate a maximum of two species or functional groups of phytoplankton, with population dynamics controlled by phosphorus (P) limitation, light requirements, and loss processes (see Table 1 for a complete list of modifiable phytoplankton parameters). Nitrogen (N) and silica (Si) species, as state variables, were added in v2 (Markelov et al., 2019). N-limited phytoplankton growth was incorporated in a recent application (Salk et al., 2022). The material cycle used by *MyLake* is presented in Appendix 1.

2.1.2. MyLake – updated model description

The assumption of lateral homogeneity in *MyLake*, inherent to most one-dimensional models, limits the model's adaptability for simulating different water column 'zones'. Consequently, in order to model the impacts of FPV we adapted and extended *MyLake* to enable simulation of the effects of varying FPV coverage on water bodies. Moreover, given the importance of phytoplankton on water supply reservoirs where FPV are often located, we enhanced the phytoplankton functionality.

2.1.2.1. Multiple tanks and exchanges between tanks. To enable the explicit simulation of FPV installations on different types of water bodies and differently functioning 'zones' of water bodies, the *MyLake* model was extended to represent water bodies in a quasi-two-dimensional way, an approach successfully applied with other freshwater models (e.g. de la Fuente and Niño, 2008; Zhang and Rao, 2012; Dimitriou et al., 2017). Specifically, the original one-dimensional (one 'tank') model structure

Table 1
MyLake Parameters describing phytoplankton functional traits. PAR is photosynthetically active radiation.

Parameter	Description
PAR saturation level for growth (mol-quanta m^{-2} s^{-1})	Controls the light-limitation of growth
Optical cross section of chlorophyll-a (m^{-2} mg^{-1})	Specifies self-shading contribution
Loss rate at 20 °C (day^{-1})	Overall loss rate (includes death, grazing etc. But not settling losses)
Settling velocity (m day^{-1})	Phytoplankton-specific settling rates
Specific growth rate at 20 °C (day^{-1})	Phytoplankton-specific maximum growth rates – modified by temperature, light and nutrient availability
Half saturation growth P concentration (mg m^{-3})	Controls shape of growth curve based upon P concentration
Half saturation growth N concentration (mg m^{-3})	Controls shape of growth curve based upon N concentration
Half saturation growth Si concentration (mg m^{-3})	Controls shape of growth curve based upon Si concentration
If phytoplankton are N-Limited	Allows specification for N-fixing phytoplankton
If phytoplankton are Si-Limited	Allows specification of Si requirement (e.g. diatoms and chrysophytes)
Scaling factor for inflow concentration of chlorophyll-a (−)	Distributes inflow chlorophyll-a across functional groups simulated

was replicated into '*n tanks*' (see supplementary information, Section 1).

The quasi-two-dimensional functionality permits each tank to be independent, allowing for variation in water body characteristics, such as depth and flow, and spatial characteristics, such as littoral and pelagic zones. Alternatively, the functionality permits the simulation of covered and uncovered zones of a water body with FPV. Flows and exchanges are specified using an eddy diffusion matrix, which governs the amount of lateral mixing between contiguous tanks and an advection matrix that specifies flows between tanks (e.g. to represent internal water body circulation patterns). While the updated *MyLake* model can simulate an unrestricted number of tanks, the computational burden and availability of data for parameterising appropriate advection and diffusion matrices could be limiting. Consequently, the number of tanks should be as parsimonious as possible given the simulation requirements (see supplementary information, Section 2).

2.1.2.2. Phytoplankton growth module. To investigate phytoplankton species composition in response to FPV and the risk to water quality, we updated the *MyLake* phytoplankton growth module to simulate an unrestricted number of phytoplankton species (or groups) with different functional behavioural traits. Here, we simulated phytoplankton in functional groups, as widely used in modelling applications, to overcome the difficulty of specifying individual species parameters (Shimoda and Arhonditsis, 2016). Specifically, we modelled diatoms, cyanobacteria and green algae, enabled by generic representations of their non-taxonomical traits known to dictate behaviour (Salmaso et al., 2015), such as growth, loss and nutrient uptake (Reynolds et al., 2002).

As nutrient limitation is a primary determinant of the abundance and species composition of phytoplankton in water bodies (O'Neil et al., 2012) we increased the model growth equations from two to three ()Eqn 1, 2 and 3). Specifically, Si species were linked to the phytoplankton dynamics equations to allow the simulations of diatoms (Harrison et al., 2012), in addition to the original phosphorus uptake module and the recently incorporated N-limited growth module (Salk et al., 2022) (see Table 1 for a complete list of phytoplankton parameters). Consequently, there are now three phytoplankton growth equations:

P limited

$$\mu = \mu_{\max} \cdot \left(\frac{S_1}{(S_1 + K_{S_1})} \right) . T_f . L_f \qquad (1)$$

P and N limited

$$\mu = \mu_{\max} \cdot \left(\frac{S_1}{(S_1 + K_{S_1})} \cdot \frac{S_2}{(S_2 + K_{S_2})} \right) . T_f . L_f \qquad (2)$$

P, N and Si limited

$$\mu = \mu_{\max} \cdot \left(\frac{S_1}{(S_1 + K_{S_1})} \cdot \frac{S_2}{(S_2 + K_{S_2})} \cdot \frac{S_3}{(S_3 + K_{S_3})} \right) . T_f . L_f \qquad (3)$$

where μ = phytoplankton species growth rate on a given day (day^{-1}), $\mu_{\max}$ is the maximum phytoplankton growth rate at 20 °C; $.T_f$ (−) is a water temperature modifier; $.L_f$ (−) is a light modifier; S_1 is phosphorus concentration (mg m^{-3}), S_2 is nitrogen concentration (mg m^{-3}), S_3 is silica concentration (mg m^{-3}), and K_{S_x} (mg m^{-3}) is the half molar saturation level for each nutrient (see Table 1 for full definitions).

2.1.2.3. Initial model testing (functionality). Testing examined the functionality of multiple tank configurations and additional phytoplankton functional group representation using data from Lake 227 (Ontario, Canada), Lake Vansjø (Norway) and subsequently Thames Water's Queen Elizabeth II reservoir (outlined below; Section 2.2.1). We tested for internal consistencies (e.g. mass-balance conservation), appropriate phytoplankton functional group behaviour and dynamics (e.g. response to nutrient concentrations (Klausmeier and Litchman, 2001) and functional group succession) and the sensitivity of model output to the number and configuration of tanks (see supplementary information, Section 2, for details).

2.2. Modelling methodology

We used the expanded model to simulate the effect of FPV on physical and biogeochemical indicators of water quality in the Queen Elizabeth II (QEII) reservoir. FPV are typically deployed on raw (untreated) water reservoirs, irrigation ponds and other artificial water bodies (Exley et al., 2021b), which typically have less extensive data than natural water bodies instrumented for research. Consequently, we took an uncertainty approach, specifically the Generalised Likelihood Uncertainty Estimation (GLUE) procedure (Beven and Binley, 1992) to account for the limited data.

2.2.1. Study location

The QEII reservoir is in south-west London (51° 23′ 27″ N, 0° 23′ 32″ W, surface area: 128 ha). The raw water reservoir has a maximum depth of 17.8 m and a maximum capacity of 19.6 million cubic meters. The reservoir is supplied with nutrient-rich water from the River Thames (Reynolds et al., 2005), pumped via three inlets on the reservoir bed, one to the west and one in each of the two southern corners. The reservoir outlet is situated in the north-eastern corner (Fig. 1). During the study year, 2018, the QEII reservoir had a mean hydraulic residence time of 44 days (Ta, 2019). Reservoir volume ranged from >95% full between January to early May, before being drawn down over the summer and autumn to 73% volume in early November. Reservoir volume then returned to >95% at the end of 2018. In 2016, a 6.3 MW capacity FPV installation was deployed on the QEII reservoir, covering ~4.5% of the reservoir's surface when full.

2.2.2. Data inputs

2.2.2.1. Forcing inputs. The QEII reservoir was modelled on a daily time step for one-year to demonstrate model application, using data from 2018. As monitoring of the QEII reservoir is conducted at the reservoir outlet, inflow nutrient concentrations were obtained from two monitoring stations on the River Thames situated upstream (Wey tributary; ~5.5 km) and downstream (Teddington Weir; ~11.5 km) of the QEII reservoir inlet (Environment Agency, 2018). Samples were taken approximately monthly and were linearly interpolated to obtain mean

Fig. 1. Conceptual Baseline 'tank' structure for QEII during 2018. Satellite image from Google Earth.

daily values throughout 2018. Inflow water temperatures were approximated from observed in-reservoir water temperatures. Daily outflow data provided by the reservoir operator were used as a proxy for inflow volume. In the absence of on-site meteorological measurements, global radiation, cloud cover, wind speed, air temperature, relative humidity, air pressure and rainfall observations from Heathrow Airport (10.5 km to the north) for 2018 were used (Met Office, 2019). Bathymetry of the QEII reservoir was digitised to 1 m intervals from a survey provided by the reservoir operator.

2.2.2.2. Data for evaluation of model performance. Observed water temperature and total chlorophyll-*a* data provided by the reservoir operator was used for model calibration and uncertainty estimation. Typically, these samples were collected weekly at the reservoir outlet at depths of 1, 3, 5, 7, 9, 11, 13 and 15 m. Weekly phytoplankton speciation, analysed by the reservoir operator, was derived from an integrated sample of the upper 1 m of the reservoir and recorded based on the cell count by ascribing a rating on an ACFOR (Abundant, Common, Frequent, Occasional, Rare) scale (see supplementary information, Section 3, for further details). Six functional groups were simulated to broadly reflect the phytoplankton species composition observed in the QEII reservoir during 2018, separated by grazed and ungrazed

groupings. The groups represent the broad functional trait differences, including grazing pressures (represented by loss rate), size, growth rate, their light requirement for growth and settling velocity. The six functional groups were reported only as *diatoms, cyanobacteria and green algae* in the following analyses (Table 2), as the grazed and ungrazed groupings were combined for each group.

2.2.3. Model geometry and simulations

2.2.3.1. Tank configuration. In this study, the new multi-tank functionality of the model was used to represent discrete zones of internal circulation. Tank configuration was based on a detailed study of internal circulation in the QEII reservoir for 2018 (Ta, 2019) and testing of tank configurations (see supplementary information, Section 2). The baseline model was assigned two tanks, one relatively short residence time, *faster-flowing tank* (70% of QEII volume) and one comparatively longer residence time, *slower-flowing tank* (30% of QEII volume). The tanks mimic the hydrologic behaviour of the QEII reservoir, namely the short-circuiting of flow between the reservoir inlets and outlet. The existing FPV array is positioned on the slower-flowing tank (Section 2.2.1; Fig. 1). The inflow and outflow of the reservoir were located in the faster-flowing tank. The distribution matrices described exchanges between the faster-flowing tank and the slower-flowing tank; lateral eddy diffusion (set at 2.5% of tank volume) and advection (set at 2.5% of tank volume) (see supplementary information, Section 2, for further details).

2.2.3.2. Identification of baseline model simulations. Acceptable baseline simulation results and parameter sets were identified by comparing model output from multiple model runs with observed data (total chlorophyll-*a*, surface temperature, stratification pattern and phytoplankton functional group proportions). Parameter ranges, comprised of all physically reasonable values for each parameter (see supplementary information, Section 3), were sampled 8000 times using a Monte Carlo strategy to limit bias within the parameter sets. Each Monte Carlo sample provided a unique set of parameters to run 8000 simulations. Each of the simulations underwent the GLUE procedure (Beven and Binley, 1992), where formalised Limits of Acceptability (LoA) were developed and used as acceptance criteria to account for the significant uncertainties associated with modelling environmental systems (see supplementary information, Section 4, for further details).

LoA were applied in the strictest sense for chlorophyll-*a* and mixed depth: any simulations that fell outside the specified limits were rejected and not used in the analyses. The remaining variables were used solely to provide additional confidence weightings. Confidence weightings (L) for accepted simulations were calculated using fuzzy weighting functions and were combined to give an overall weighting for each simulation. Chlorophyll-*a* (L_{Chl}), mixed depth (L_{mxd}) and water temperature (L_{wt}) were equally weighted in the combined overall goodness of fit weighting (Wt). Phytoplankton functional groups, where L_D, L_G and L_C are the weighting for diatoms, cyanobacteria and green algae, respectively, had a weighting of one-third to prevent over-constraint on

Table 2
Nominal phytoplankton functional groups used and descriptive functional traits. See supplementary information, Section 3, for the ranges of each sampled parameter.

Phytoplankton functional group	Nutrient limited			Size	Growth Rate	Light requirement for growth	Settling velocity	Loss rate
	P	N	Si					
Diatoms – *ungrazed*	✓	✓	✓	Large	Slow	Low	High	–
Diatoms – *grazed*	✓	✓	✓	Large	Slow	Low	High	+
Cyanobacteria – *ungrazed*	✓			Small/medium	Medium	Medium	Very low	–
Cyanobacteria – *grazed*	✓			Small/medium	Medium	Medium	Very low	+
Green/other algae – *ungrazed*	✓	✓		Small	Fast	Medium	Low	–
Green/other algae – *grazed*	✓	✓		Small	Fast	Medium	Low	+

+: Increased to reflect grazing losses; −: Reduced to reflect no grazing losses.

functional groups (Eqn 4).

$$Wt = [(L_{Chl} + L_{mxd} + L_{wt} + (L_D.0.33) + (L_C.0.33) + (L_G.0.33))] \quad (4)$$

As all acceptable simulations are deemed to represent the system behaviour (given the available data), they are all used to represent the baseline. However, as each acceptable simulation is associated with a goodness of fit weighting, which is propagated to the final results, each acceptable simulation contributes differently. Using all the acceptable simulations in this way explicitly propagates all known modelling uncertainties to final modelling results. The implementation of FPV deployment in the model took the form of a modification to each of the acceptable parameter sets to represent the solar array associated with the scenario of interest.

2.2.3.3. FPV deployment scenarios. Three 'deployment scenarios' were run to investigate the impact of array siting location on water body response (Table 3). Each scenario was run multiple times to simulate varying degrees of FPV coverage – the 'coverage increments'. The coverage increment represents the percentage of the reservoir's total surface area covered by FPV, accounting for the existing 4.5% coverage of the presently deployed array (see Section 2.2.1). In the following scenarios, we use coverage increments of 10% from a baseline of 0% coverage to complete reservoir coverage (100%).

- Each deployment scenario was simulated with a range of FPV 'coverage increments' from 0% coverage (baseline) to 100% in 10% increments.

2.3. Modelling assumptions and sources of uncertainty

Each model run, in terms of the deployment scenario and coverage increment, was based on a set of assumptions to represent the water body and approximate the effects of FPV coverage. At present, there are no published values for the effect of FPV on air temperature, wind speed and incoming solar radiation at the air-water interface. The effect on each driver is likely modified depending on system design, such as transparency of the PV module, airflow beneath the floating array and orientation of the array (Armstrong et al., 2020; Exley et al., 2021a; Ziar et al., 2021). For this study, the effects of an array were estimated from unpublished observations made at an FPV installation (see supplementary information, Section 5, for methods) and published observations made at a ground-based installation (Armstrong et al., 2016). Based on the results of these preliminary observations, we assumed that between the water's surface and the underside of the PV module; air temperature is warmed by 8%, incoming solar radiation is reduced by 94%, and wind speed is reduced by 95%. All scenarios are also based on the likely assumptions that the functional phytoplankton groups adequately

Table 3
Scenarios and a summary of the deployment configuration.

Scenario	Description
Baseline	*The reservoir simulated with no additional FPV coverage (includes the existing 4.5% coverage of the presently deployed array) – shown as 0% coverage.*
Scenario-Fast	FPV installation initially deployed on the faster-flowing tank, an area of the reservoir with a shorter-residence time. Once the FPV installation exceeds the area of the faster-flowing tank the FPV array is deployed upon the slower-flowing tank (Fig. 1).
Scenario-Slow	FPV installation initially deployed on the slower-flowing tank, an area of the reservoir with a longer-residence time. Once the FPV installation exceeds the area of the slower-flowing tank the FPV array is deployed upon the faster-flowing tank (Fig. 1).
Scenario-Central	Central siting of FPV installation. Initially the array is deployed on the faster-flowing tank, as the larger of the two tanks (Fig. 1). Once the remaining uncovered area of the faster-flowing tank is equal in area to the slower-flowing tank, the deployment of the array is split equally between each tank.

represent the phytoplankton community observed in the QEII reservoir and that the initial phytoplankton community composition (i.e., relative proportions of taxa) were set to be equal on the first day of each simulation to permit an equal chance of proliferation.

2.4. Model output analysis

To summarise the impact of varying FPV coverage and siting location on phytoplankton biomass and species composition, we compared model outputs from each scenario against the baseline (Table 3). We analysed the output from the faster-flowing tank, as this is the tank that feeds the water treatment works. Given the plethora of data outputted, we focussed on variables influencing phytoplankton biomass and species composition, including surface water temperature at 1 m and stratification metrics. To represent phytoplankton biomass and species composition, we used total chlorophyll-*a* concentration and the proportions of each phytoplankton functional group as a proportion of total chlorophyll-*a*, both at 1 m depth. The proportions of phytoplankton functional groups are presented as relative, not absolute values for visual clarity.

Given the use of the GLUE methodology, each scenario has the outputs from several model simulations. To capture the variability in outcomes, thus representing the uncertainty, we use the median, 2.5th and 97.5th percentiles, thus providing the average outcome and the 95% confidence interval. To explore the impacts on the annual minimum (T_{min}) and maximum (T_{max}) water temperature and maximum total chlorophyll-*a* concentration, we use the mean of each based on a ten-day window defined by the baseline model runs. Stratification was determined using a threshold density gradient of 0.1 kg m^{-3} m^{-1} between adjacent layers (Gray et al., 2020). Two metrics were used to summarise stratification duration. These were continuous stratification, the longest period of stratification in each simulation, and cumulative stratification duration, the total number of stratified days during the one-year simulation period. Stratification onset and overturn were defined as the first and last day of the longest period of continuous stratification, respectively.

3. Results

3.1. Simulations within the limits of acceptability

Seventy-five parameter sets were within the LoA for all simulations; the remaining 7925 parameter sets were rejected and not used in the subsequent analyses. Given the limited input data and strict inclusion criteria applied, most excluded parameter sets were rejected based on their representation of total chlorophyll-a (Fig. 2), functional groups and mixed depth. The model simulated water temperature within the LoA for most parameter sets (<95%). The goodness of fit weighting for the accepted parameter sets ranged from 80.62 to 84.01, of a maximum possible weighting of 204 (determined by the number of observations available for the QEII reservoir).

3.2. Response of thermal properties

FPV coverage cooled median surface water temperatures throughout the year (Figures S 6–1, 6–2, 6–3). However, on a small number of days between mid-spring and early summer, the 10% coverage increment resulted in slightly warmer (<0.6 °C) surface water temperatures than the baseline (i.e. no additional FPV coverage) in Scenario-Fast and Scenario-Central for nine days. Similarly, at 10–30% coverage in Scenario-Slow, there were ten days when FPV coverage warmed median surface water temperatures (<0.5 °C) compared to the baseline.

For all scenarios, median T_{max} and T_{min} were reduced with increasing FPV coverage, based on the mean of a window (± five days), defined by the baseline model runs. FPV deployment on the fast-flowing tank (Scenario-Fast) saw a comparatively quick decline in T_{max} and T_{min} with
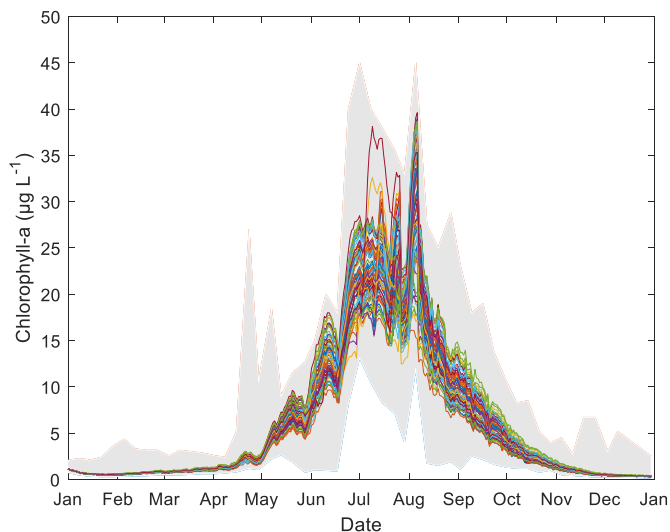
Fig. 2. Simulated chlorophyll-a (coloured lines) samples within the limits of acceptability (grey shaded area).

increasing FPV coverage. Median T_{max} decreased on average 0.55 ± 0.09 °C (mean difference $\pm$ *SD*; hereafter unless stated) per 10% coverage increment for FPV coverages up to 70% (i.e. when the FPV encroached on the slower flowing tank). Median T_{min} decreased by 0.20 ± 0.11 °C per 10% coverage increment up to 70% coverage. The rate was reduced once the array encroached on the slower-flowing tank (FPV coverages greater than 70%). T_{max} decreased by 0.16 ± 0.03 °C per 10% coverage increment and T_{min} decreased by 0.02 ± 0.004 °C per 10% coverage increment (Fig. 3a and b).

Deployment on the slower-flowing tank (Scenario-Slow) initially caused a slower decline in median T_{max} and T_{min}, 0.15 ± 0.04 °C and 0.02 ± 0.01 °C, respectively, per 10% coverage increment up to 30%, than in Scenario-Fast. After the FPV encroached on the faster-flowing area (above 30% coverage), T_{max} decreased by 0.56 ± 0.15 °C, and T_{min} decreased by 0.20 ± 0.11 °C, per 10% coverage increment. In contrast, median T_{max} declined linearly by 0.44 ± 0.08 °C for each 10% coverage increment when the array was located centrally on the reservoir (Scenario-Central; Fig. 3a). T_{min} for Scenario-Central reduced by 0.14 ± 0.06 °C for each 10% increase in FPV coverage. There was increasing divergence between the lower (2.5th) and upper (97.5th) percentile at higher FPV coverages (Fig. 3b). For example, at 10% coverage the range between the lower and upper percentile was 0.65 °C, this increased to 0.70 °C at 50% and 0.94 °C at 90% FPV coverage.

In response to increasing array coverage, continuous and cumulative stratification duration decreased rapidly when the array was deployed on the faster-flowing tank or centrally (Scenario-Fast and Scenario-Central; Fig. 3c and d). Maximum stratification duration was up to 22 days longer in Scenario-Slow than under Scenario-Fast at 30% FPV coverage (Fig. 3c). Cumulative stratification duration was up to 75 days longer in Scenario-Slow than under Scenario-Fast at 30% FPV coverage (Fig. 3d). Significant stratification events did not occur in Scenario-Fast and -Central when array coverage exceeded 50% and in Scenario-Slow when coverage exceeded 70% (Fig. 3c and d). See supplementary information, Section 9, for the number of stratified simulations at each FPV coverage.

The relationships between FPV coverage and stratification onset and overturn were weaker than for stratification duration (Fig. 3e and f). Stratification onset generally shifted to later in the year with FPV coverages of up to 40% for Scenario-Fast and -Central (Fig. 3e). However, some simulations had an earlier onset of stratification at the 10% FPV coverage increment. In Scenario-Slow, stratification onset showed a weak shift to later in the year with FPV coverages of up to 70% (Fig. 3e). However, a few Scenario-Slow simulations showed an earlier onset at

10–40% FPV coverage than the baseline (Fig. 3e).

The overturn of stratification did not have a clear trend with increasing FPV coverage. However, overall, there was a tendency for overturn to be slightly later for all three scenarios than the baseline (Fig. 3f). However, a small number of simulations showed earlier overturn than the baseline (Fig. 3f). For example, at 10 and 20% FPV coverage, the lower extent of the estimated range was earlier than the lower extent of the baseline range for Scenario-Fast and Scenario-Central (Fig. 3f). Overturn of stratification in Scenario-Slow did not have a clear trend with increasing coverage, although typically it occurred slightly earlier than in Scenario-Fast and Scenario-Central at FPV coverages 20% or greater (Fig. 3f). Overturn occurred earlier than the baseline in a small number of simulations, for example, at 10–40% FPV coverage, when only the slower-flowing tank was covered.

3.3. Response of phytoplankton

3.3.1. Total chlorophyll-a

In Scenario-Fast and Scenario-Central maximum total chlorophyll-a concentration, based on the mean of a window ($\pm$ five days), defined by the baseline model runs, declined exponentially with increasing FPV coverage (Fig. 4). For example, in Scenario-Fast, median total chlorophyll-a was reduced by 10.21 µg L^{-1} at 10% FPV coverage, 20.40 µg L^{-1} at 50% and 22.09 µg L^{-1} at 90% compared to the baseline scenario. Each additional 10% coverage increment, up to 60%, reduced median total chlorophyll-a by 3.59 ± 1.84 µg L^{-1} on average (Fig. 4). Coverages exceeding 60% in Scenario-Fast had negligible total chlorophyll-a (<1 µg L^{-1}).

Comparatively, Scenario-Central showed a slightly smaller reduction in median total chlorophyll-a concentration than Scenario-Fast. For example, median total chlorophyll-a was reduced by 4.01 µg L^{-1} at 10% FPV coverage, 19.69 µg L^{-1} at 50% and 22.01 µg L^{-1} at 90% compared to the baseline scenario. In Scenario-Central, each additional 10% FPV coverage increment, up to 70%, reduced median total chlorophyll-a by 3.05 ± 2.11 µg L^{-1} (Fig. 4). Coverages exceeding 70% in Scenario-Central had negligible total chlorophyll-a (<1 µg L^{-1}).

In Scenario-Slow, total chlorophyll-a concentration generally reduced with increasing FPV coverage. However, at lower FPV coverages (10–30% coverage) where only the slower-flowing tank was covered, total chlorophyll-a simulations showed both increases and decreases from the baseline (Fig. 4). At 10% FPV coverage, total chlorophyll-a was either reduced by up to 5% (0.89 µg L^{-1}; 2.5th percentile) or increased by up to 28% (7.95 µg L^{-1}; 97.5th percentile). At 20% FPV coverage, total chlorophyll-a either reduced by up to 15% (2.52 µg L^{-1}; 2.5th percentile) or increased by up to 15% (4.28 µg L^{-1}; 97.5th percentile). At 30% FPV coverage, total chlorophyll-a either reduced by up to 19% (3.23 µg L^{-1}; 2.5th percentile) or increased by up to 4% (1.02 µg L^{-1}; 97.5th percentile). Above 30% FPV coverage, when the faster-flowing tank started to be covered, median total chlorophyll-a declined on average by 2.87 ± 2.35 µg L^{-1} per 10% additional cover.

3.3.2. Annual total chlorophyll-a

Median total chlorophyll-a generally reduced with increasing FPV coverage throughout the year for all scenarios (Fig. 5 and supplementary information, Section 7, for 95% confidence interval). However, on a small number of days between late May and the end of July, median total chlorophyll-a was greater than the baseline in Scenario-Slow at 10–30% FPV coverage. FPV coverage had the greatest relative impact on median total chlorophyll-a at the start of August (Figure S 7–1). For example, at 10% FPV coverage median total chlorophyll-a had a relative reduction of 48% (24.38 µg L^{-1}) in Scenario-Fast and Scenario-Central. Whilst in Scenario-Slow, the greatest relative difference for 10% FPV coverage occurred in early June; a 17% (2.09 µg L^{-1}) reduction compared to the baseline scenario. The absolute differences as coverage exceeded 70% in Scenario-Fast and Scenario-Central were relatively small compared to lower coverages when the array was deployed
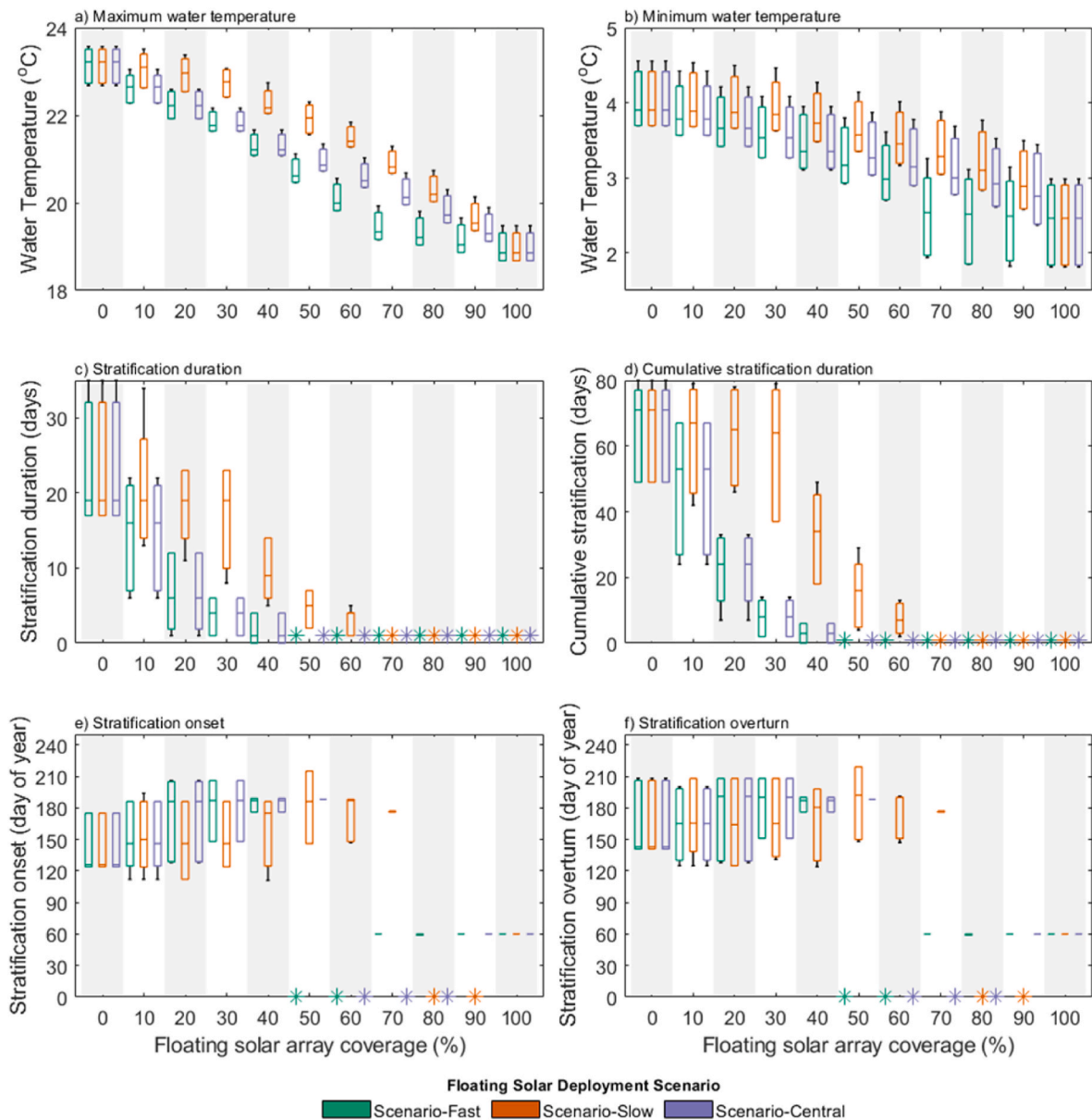
Fig. 3. A) Annual maximum and b) minimum water temperature, c) stratification duration, d) cumulative stratification duration, and stratification e) onset and f) overturn day, versus floating solar (FPV) array coverage for each deployment scenario. An asterisk indicates no prolonged stratification event occurred for the simulation. Whiskers represent the minimum and maximum of the simulation results presented. The box represents the 2.5th & 97.5th percentiles, which gives a 95% confidence interval that simulation estimates fall within this range. 0% FPV coverage represents QEII reservoir simulated as a baseline with no additional FPV coverage.

exclusively on the faster-flowing tank (Fig. 5). The opposite occurred for Scenario-Slow, with coverages up to 30%, the area of the slower-flowing tank, having a small absolute difference with the baseline. The absolute difference increased once the array started to cover the faster-flowing tank (Fig. 5).

3.3.3. Phytoplankton functional group dynamics

While simulated chlorophyll-*a* concentrations declined exponentially with increasing coverage, the relative proportion of phytoplankton functional groups varied. In Scenario-Fast, at FPV coverages of up to 60%, diatoms dominated for most of the year, with their dominance increasing as FPV coverage increased up to 40% (Fig. 6 and Figure S8–1). As the coverage increased above 60%, proportions of green algae increased, approaching a similar proportion as diatoms. In some cases, green algae were very similar to, or slightly exceeded, the proportions of diatoms towards the end of summer, as for the baseline

scenario (Fig. 6).

Similarly, diatoms increasingly dominated with FPV coverages of up to 70% in Scenario-Central. Diatom dominance slowly reduced from 70% to 100% coverage, associated with a higher proportion of green algae (Figure S8–2). In Scenario-Slow, FPV coverages of up to 90% were associated with diatoms dominating for most of the year (Figure S8–3). Diatom dominance strengthened as FPV coverage increased over 40% but declined again over 70%. In some cases, typically at FPV coverages up to 30%, green algae were very similar to, or slightly exceeded, the proportions of diatoms towards the end of summer, as they did in the baseline scenario (Figure S8–3). Cyanobacteria did not have a high relative or absolute abundance regardless of FPV coverage.

4. Discussion

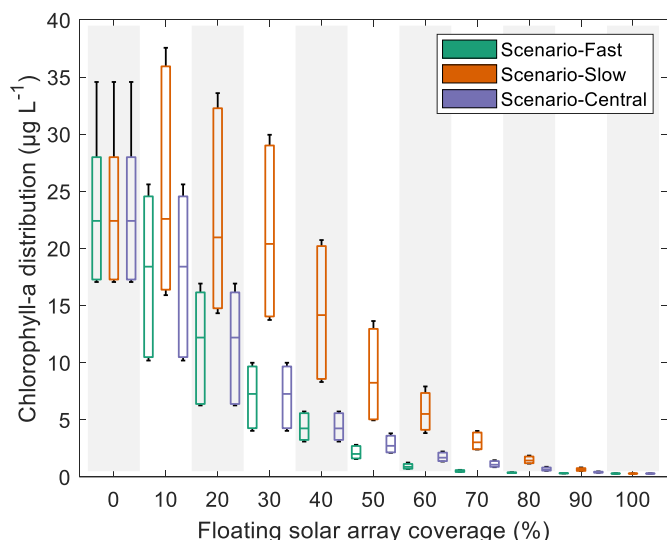We found reduced phytoplankton biomass and changes in species

Fig. 4. Total chlorophyll-a (based on the mean of a window, ± five days, around the day of maximum total chlorophyll-a) versus floating solar array coverage. Whiskers represent the minimum and maximum of the simulation results presented. The box represents the 2.5th & 97.5th percentiles, which gives a 95% confidence interval that simulation estimates fall within this range. 0% floating solar coverage represents QEII reservoir simulated as a baseline.

composition can be directly attributed to the direct shading effects from reduced solar radiation and indirect mixing effects from wind sheltering of FPV. We also found that the different thermal dynamics associated with each siting location meant phytoplankton in the faster flowing tank appear more sensitive to low FPV coverage than the phytoplankton in the slower flowing tank, as they have to contend with both shading and rapid flushing, resulting in a large cumulative effect. Inflow volume, water temperature and nutrient inputs remained unchanged. In general, increased FPV coverage reduced total chlorophyll-a, although the

absolute and relative reduction varied between each FPV deployment siting location scenario. There were a small number of simulations where phytoplankton biomass increased when the array was deployed on the slower flowing area of the reservoir. However, these increases were time-limited and only at array coverages of up to 30% in a small number of simulations.

4.1. Drivers behind the reduced phytoplankton biomass

We found that minimum, maximum and median surface water temperatures cooled due to the shading effects of FPV, slowing phytoplankton growth by reducing metabolic rates (Kraemer et al., 2017) as FPV coverage increased. As growth rates are species-specific, varying with cell size, each functional group responded uniquely to cooler water temperatures owing to increasing FPV cover (Reynolds, 2006). While deployment location had several complex and interacting effects, the effects of higher flow speed combined with FPV coverage led to an enhanced cooling effect. Given this flushing effect, the faster circulation tank exhibited a greater reduction in total chlorophyll-*a* and a more pronounced change in phytoplankton community structure than for similar coverages of FPV deployed on the slower circulation tank.

The cooler water temperatures associated with increasing FPV coverage reduced continuous and cumulative stratification duration. This indirect effect of FPV on reservoir mixing contributed to lower total chlorophyll-*a* in the reservoir (Exley et al., 2021a). In the absence of stratification or a shorter stratified period, the mixed layer, a fundamental driver of phytoplankton growth (Ross and Sharples, 2008; Longhi and Beisner, 2009), is deeper or fully mixed. The deepening of the mixed layer worsens the effective light climate for phytoplankton, moving them further from the higher light intensity surface waters (Reynolds, 1997). However, non-stratified conditions may allow phytoplankton to access pools of nutrients in the lower water column, favouring those species tolerant of the lower light availability at depth. On the small number of days when total chlorophyll-a increased with FPV coverage, the sheltering effect at the air-water interface likely
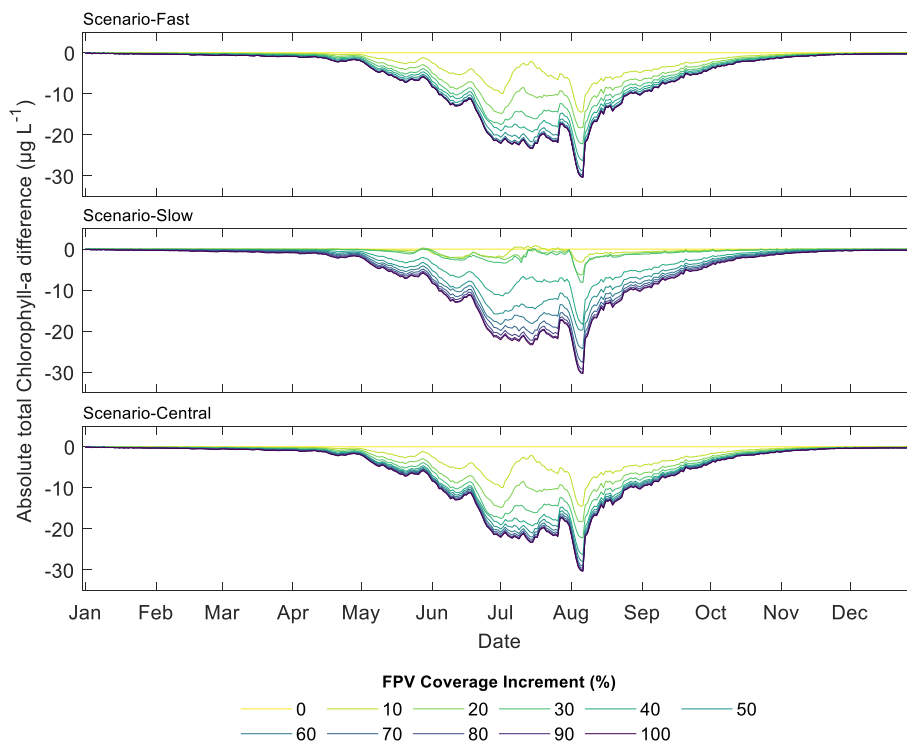

Fig. 5. Annual median total chlorophyll-a absolute difference by scenario. 0% floating solar coverage represents QEII reservoir simulated as a baseline with no additional floating solar coverage. The relative difference in chlorophyll-a is shown in Figure S 7–1.
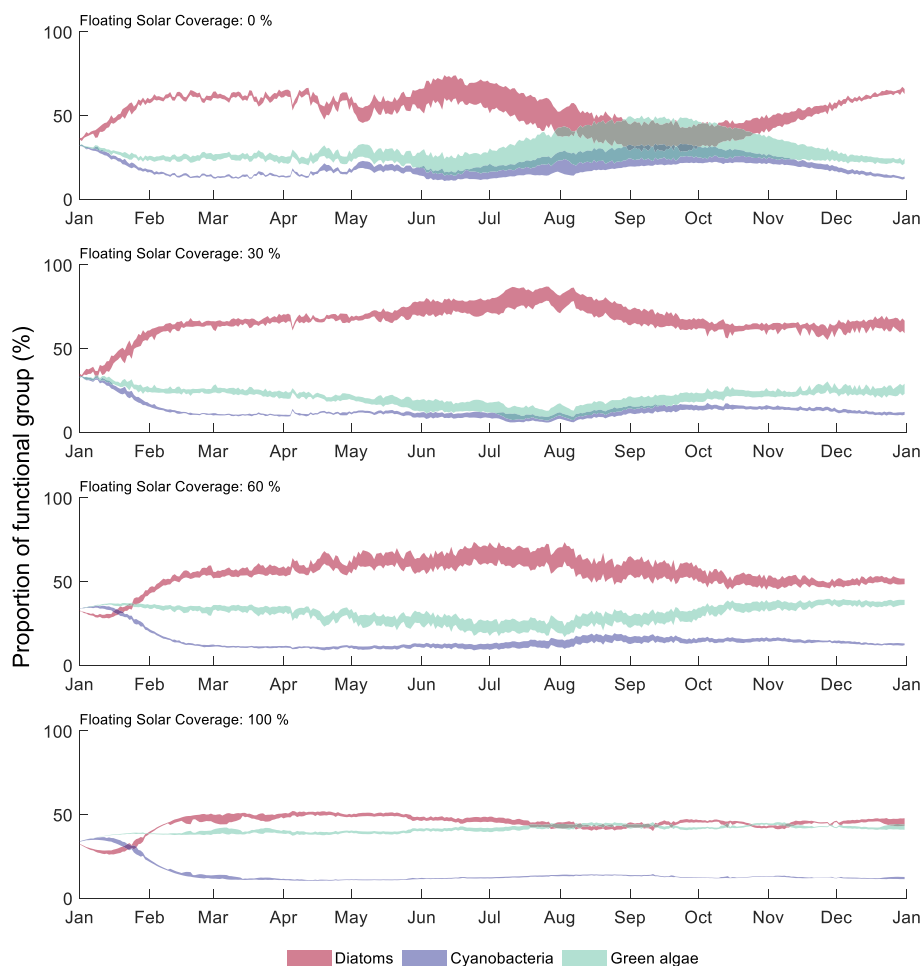
Fig. 6. Scenario-Fast: Proportion of phytoplankton functional groups as a percentage of total chlorophyll-a for the simulated period. The initial phytoplankton functional group proportions were set evenly, therefore, the first 30 days of simulations are model run-in time and should be ignored. 0% floating solar coverage represents QEII reservoir simulated as a baseline.

reduced mixing, improving the conditions for phytoplankton growth (Exley et al., 2021a).

4.2. The consequences for phytoplankton functional-type dynamics

Modifications to reservoir thermal properties and shading from FPV coverage resulted in changes to phytoplankton functional-type dynamics, with the different siting locations modifying the response. Generally, the relative dominance of diatoms increased in the autumn with moderate FPV coverages as green algae populations reduced. However, these changes were offset by the overall rapid decline in phytoplankton biomass associated with increasing FPV coverage. In the faster circulation scenario, as FPV coverage increased and the reservoir became more mixed, dominance switched from green algae to diatoms, consistent with their affinity to well-mixed water bodies (Jäger et al., 2008). In the slower circulation scenario, which experienced less of a reduction in stratification duration than the faster circulation scenario, species composition remained similar to the baseline conditions.

Importantly, given the implications for water treatment and reservoir recreational use, cyanobacteria dominance did not increase with increasing FPV coverage for any of the deployment scenarios. This is attributable to the shaded conditions and additionally, the more mixed water column reduced the ability of cyanobacteria to regulate their buoyancy and vertical position to obtain favourable light and nutrient conditions (Reynolds et al., 1987; Burkholder, 2009). However, whilst our simulations show a reduction in total cyanobacteria biomass with increasing FPV coverage relative to the baseline, our use of

functional-type aggregates may overlook the specific traits, tolerances and sensitivities among cyanobacteria taxa which could allow individual shade-tolerant or lower-optimum temperature species to dominate (Carey et al., 2012; Mantzouki et al., 2016; Armstrong et al., 2020). Studies considering the effects of surface covers have shown a switch to cyanobacteria dominance in some instances (Yamamichi et al., 2018; Exley et al., 2021b). However, the expanded model can simulate an unrestricted number of phytoplankton species, so assuming sufficient input data and observations to constrain the model, this uncertainty could be reduced in future applications.

4.3. FPV as a tool for water body management

Our results suggest that water body managers could tailor FPV system design and siting location to achieve the management goals of the host water body. The impact of percentage cover is clear, with opportunities for tailoring reductions to water temperature, mixing dynamics and phytoplankton biomass and species composition. Further, the interaction between the different residence times associated with each scenario and increasing FPV coverage shows that siting location is an important consideration when planning the deployment of an FPV array. Modifying FPV siting location between areas of different circulation can contribute greater water quality co-benefits while using identical FPV coverage. For example, deploying an FPV array covering 40% of the reservoir on the faster-flowing tank reduced total chlorophyll-*a* by up to 2.9 times more than deploying the same size array on the slower-flowing tank. Whilst the primary objective of an FPV installation is to generate

renewable electricity, the potential for non-energy water quality co-benefits could offer an additional incentive to water body managers (de Lima et al., 2021; Exley et al., 2021a). However, this should be tested empirically given the simplification of the water body into faster and slower flowing tanks.

Regardless of deployment location, the large, sustained reductions in phytoplankton with FPV deployment may provide an alternative to hydrological manipulation in reservoirs. Typically, reservoirs used for drinking water are managed to limit thermal stability, impeding the development of stratification and subsequent phytoplankton growth, which can be detrimental to water quality and disrupt the water treatment process (Paerl, 2014; Visser et al., 2015; Huisman et al., 2018). Currently, management techniques that attract capital and operational expenditure, including flushing and artificial mixers, are used to change the system's hydrology or light regime for phytoplankton (Visser et al., 2015). Alternatively, FPV provides an opportunity to overcome the growing challenge of managing phytoplankton blooms (Burkholder, 2009; Paerl et al., 2019; Plaas and Paerl, 2021), negating the need for such reservoir management and also generating zero-carbon electricity.

However, there may be undesirable consequences of FPV deployment, especially for reservoirs used for recreation (e.g. the obstruction of the water's surface) or those supporting aquatic life. Phytoplankton are the primary source of energy in lake food webs (Kalff, 2002) and an important component of global biogeochemical cycles (Falkowski, 1994). Consequently, FPV induced changes could have profound ecological impacts. For example, lake production is a significant driver of zooplankton species richness (Hessen et al., 2006) and the disruption to trophic cascades may cause a significant reduction in planktivorous fish (Jeppesen et al., 2002; Gerdeaux et al., 2006). Therefore, practitioners should undertake careful planning to ensure deployments and their corresponding impact on phytoplankton aligns with the management goals of the host water body, with consideration for all trophic levels and accounting for the full range of plausible outcomes across the 95% confidence interval as determined by the GLUE methodology.

4.4. Expanded model adequacy, application and critical research needs

This study has provided novel model insights into FPV impacts unobtainable through field manipulation. The expanded model allows the explicit simulation of FPV installations on different types of water bodies and differently functioning tanks of water bodies. The expanded model remains computationally efficient, thus allowing multiple runs to capture uncertainty, given the nature of the data commonly available for the water bodies FPV tend to be deployed on. The functionality to simulate discrete zones of water bodies will allow further research questions pertinent to the deployment of FPV to be answered. For example, determining the influence of water body morphometric characteristics (e.g. depth and surface area) and FPV deployment layout (i.e. one continuous array or multiple smaller arrays) on FPV water quality impacts. Moreover, it will allow the implications of geographical location and future climate to be simulated. As understanding of FPV impacts and field data collection advance, future modelling studies will need to focus on the performance of critical processes in the model, for example, horizontal wind mixing. Moreover, the suitability of different models, which range in their complexity, will need to be assessed in light of the water body characteristics, including size, and research aims.

Enhanced phytoplankton representation to simulate species composition enables the model to assess phytoplankton response in more detail. Better resolution of phytoplankton impacts is critical given the impacts of climate change and the implications for water supply reservoirs. In particular, the linking of Si species to the phytoplankton dynamics equations allows the representation of diatoms that can adversely affect water treatment as filamentous species block filters.

Application of the GLUE methodology provides insightful model outcomes (e.g. a 95% confidence interval for simulations) despite the sparser data inputs than desirable for water body modelling. High

frequency and spatially explicit monitoring of water quality impacts at existing FPV installations are required to constrain the model better and reduce uncertainties in estimated responses. Ideally, studies should consider a BACI (Before, After, Control, Impact) design (Stewart-Oaten et al., 1986), to monitor water body response before and after FPV deployment, using a control to ensure any observed impacts are specific to the intervention. Such observations will provide an empirical assessment of model outcomes and more robust modelling representations of change. Further, given the importance of phytoplankton communities to water body function and the implications for water treatment, detailed quantitative phytoplankton speciation data would be invaluable to constrain the model better and improve phytoplankton functional group representations.

5. Conclusion

FPV deployment continues rapidly worldwide, outpacing understanding of any concomitant environmental impacts. Our findings demonstrate that modelling, using an uncertainty framework, can provide useful insight into possible water body response. Specifically, we found that FPV generally promotes cooler water temperatures that, coupled with deteriorated light conditions, slow phytoplankton growth. A less favourable mixing regime with FPV coverage can also lead to substantial phytoplankton biomass reductions, even with only a small percentage of a reservoir covered by FPV. FPV deployment also changes phytoplankton community composition, but any negative consequences were negated by the considerable reductions in total biomass, allaying hypothesised water quality concerns of a switch to undesirable species.

Moreover, our results show that the location of an FPV on the water surface can significantly affect water body thermal dynamics, modifying phytoplankton response beyond the impacts of percentage coverage. This outcome demonstrates the need to consider spatial location within the water body in addition to the total magnitude of FPV coverage for deployment decisions. Modelling approaches present a valuable and resource-efficient tool to explore water body-FPV interactions, enabling the assessment of FPV design and location options without the need for extensive *in-situ* testing. Pre-deployment modelling thus could help FPV developers and water body managers minimise negative impacts and maximise co-benefits of FPV across a range of targeted water bodies worldwide.

Author's contributions

Giles Exley: Conceptualization, Formal analysis, Investigation, Software, Methodology, Validation, Writing – original draft, Writing – review & editing, Visualisation; **Trevor Page:** Conceptualization, Formal analysis, Investigation, Software, Methodology, Validation, Writing – review & editing, Supervision; **Stephen J. Thackeray:** Conceptualization, Methodology, Writing – review & editing; **Andrew M. Folkard:** Conceptualization, Methodology, Writing – review & editing, Supervision; **Raoul-Marie Couture**: Conceptualization, Methodology, Writing – review & editing, Resources; **Rebecca R. Hernandez:** Writing – review & editing, Supervision; **Alexander E. Cagle:** Investigation, Writing – review & editing; **Kateri R. Salk:** Methodology, Software, Writing – review & editing; **Lucie Clous:** Software, Writing – review & editing; **Peet Whittaker:** Software, Writing – review & editing; **Michael Chipps:** Methodology, Writing – review & editing; **Alona Armstrong:** Conceptualization, Methodology, Writing – review & editing, Supervision, Funding acquisition, Resources.

Declaration of competing interest

The authors declare that they have no known competing financial interests or personal relationships that could have appeared to influence the work reported in this paper.

Data availability

Data will be made available on request.

Appendix A. Supplementary data

Supplementary data to this article can be found online at https://doi.org/10.1016/j.jenvman.2022.116410.

References

Armstrong, A., Ostle, N.J., Whitaker, J., 2016. Solar park microclimate and vegetation management effects on grassland carbon cycling. Environ. Res. Lett. 11 (7).

Armstrong, A., Page, T., Thackeray, S.J., Hernandez, R.R., Jones, I.D., 2020. Integrating environmental understanding into freshwater floatovoltaic deployment using an effects hierarchy and decision trees. Environ. Res. Lett. 15 (11).

Beven, K., Binley, A., 1992. The future of distributed models - model calibration and uncertainty prediction. Hydrol. Process. 6 (3), 279–298.

Burkholder, J.M., 2009. Harmful algal blooms. In: Likens, G.E. (Ed.), Encyclopedia of Inland Waters. Academic Press, Oxford, pp. 264–285.

Cagle, A.E., Armstrong, A., Exley, G., Grodsky, S.M., Macknick, J., Sherwin, J., Hernandez, R.R., 2020. The land sparing, water surface use efficiency, and water surface transformation of floating photovoltaic solar energy installations. Sustainability 12 (19).

Carey, C.C., Ibelings, B.W., Hoffmann, E.P., Hamilton, D.P., Brookes, J.D., 2012. Eco-physiological adaptations that favour freshwater cyanobacteria in a changing climate. Water Res. 46 (5), 1394–1407.

Chapra, S.C., Boehlert, B., Fant, C., Bierman Jr., V.J., Henderson, J., Mills, D., Mas, D.M. L., Rennels, L., Jantarasami, L., Martinich, J., Strzepek, K.M., Paerl, H.W., 2017. Climate change impacts on harmful algal blooms in U.S. Freshwaters: a screening-level assessment. Environ. Sci. Technol. 51 (16), 8933–8943.

Choi, Y.-K., Lee, N.-H., Kim, K.-J., 2013. Empirical research on the efficiency of floating PV systems compared with overland PV systems. Proceedings, The 3rd International Conference on Circuits, Control, Communication, Electricity, Electronics, Energy, System, Signal and Simulation 284–289.

Danilov, R.A., Ekelund, N.G.A., 2001. Phytoplankton communities at different depths in two eutrophic and two oligotrophic temperate lakes at higher latitude during the period of ice cover. Acta Protozool. 40 (3), 197–201.

de la Fuente, A., Niño, Y., 2008. Pseudo 2D ecosystem model for a dendritic reservoir. Ecol. Model. 213 (3–4), 389–401.

de Lima, R.L.P., Paxinou, K., C Boogaard, F., Akkerman, O., Lin, F.-Y., 2021. In-situ water quality observations under a large-scale floating solar farm using sensors and underwater drones. Sustainability 13 (11).

Dimitriou, E., Ntoanidis, L., Bellos, V., Papadaki, C., 2017. Comparison of West Balkan adult trout habitat predictions using a Pseudo-2D and a 2D hydrodynamic model. Nord. Hydrol 48 (6), 1697–1709.

Environment Agency, 2018. Water quality archive. Available at: https://environment.data.gov.uk/water-quality/view/landing. Accessed: 16/02/21.

Exley, G., Armstrong, A., Page, T., Jones, I.D., 2021a. Floating photovoltaics could mitigate climate change impacts on water body temperature and stratification. Sol. Energy 219, 24–33.

Exley, G., Hernandez, R.R., Page, T., Chipps, M., Gambro, S., Hersey, M., Lake, R., Zoannou, K.S., Armstrong, A., 2021b. Scientific and stakeholder evidence-based assessment: ecosystem response to floating solar photovoltaics and implications for sustainability. Renew. Sustain. Energy Rev. 152, 111639.

Falkowski, P.G., 1994. The role of phytoplankton photosynthesis in global biogeochemical cycles. Photosynth. Res. 39 (3), 235–258.

Gerdeaux, D., Anneville, O., Hefti, D., 2006. Fishery changes during re-oligotrophication in 11 peri-alpine Swiss and French lakes over the past 30 years. Acta Oecologica-International Journal of Ecology 30 (2), 161–167.

Gorjian, S., Sharon, H., Ebadi, H., Kant, K., Scavo, F.B., Tina, G.M., 2021. Recent technical advancements, economics and environmental impacts of floating photovoltaic solar energy conversion systems. J. Clean. Prod. 278, 124525.

Gray, E., Mackay, E.B., Elliott, J.A., Folkard, A.M., Jones, I.D., 2020. Wide-spread inconsistency in estimation of lake mixed depth impacts interpretation of limnological processes. Water Res. 168, 115136.

Grizzetti, B., Liquete, C., Pistocchi, A., Vigiak, O., Zulian, G., Bouraoui, F., De Roo, A., Cardoso, A.C., 2019. Relationship between ecological condition and ecosystem services in European rivers, lakes and coastal waters. Sci. Total Environ. 671, 452–465.

Haas, J., Khalighi, J., de la Fuente, A., Gerbersdorf, S.U., Nowak, W., Chen, P.J., 2020. Floating Photovoltaic Plants: Ecological Impacts versus Hydropower Operation Flexibility, vol. 206. Energy Conversion and Management, 112414.

Harrison, J.A., Frings, P.J., Beusen, A.H.W., Conley, D.J., McCrackin, M.L., 2012. Global importance, patterns, and controls of dissolved silica retention in lakes and reservoirs. Global Biogeochem. Cycles 26 (2).

Haugwitz, F., 2020. *Floating solar PV gains global momentum*: PV Magazine. Available at: https://www.pv-magazine.com/2020/09/22/floating-solar-pv-gains-global-momentum/. Accessed: 02/05 2021.

Hessen, D.O., Faafeng, B.A., Smith, V.H., Bakkestuen, V., Walseng, B., 2006. Extrinsic and intrinsic controls of zooplankton diversity in lakes. Ecology 87 (2), 433–443.

Hipsey, M.R., Bruce, L.C., Boon, C., Busch, B., Carey, C.C., Hamilton, D.P., Hanson, P.C., Read, J.S., de Sousa, E., Weber, M., Winslow, L.A., 2019. A General Lake model (GLM 3.0) for linking with high-frequency sensor data from the global lake ecological observatory network (GLEON). Geosci. Model Dev. (GMD) 12 (1), 473–523.

Ho, J.C., Michalak, A.M., Pahlevan, N., 2019. Widespread global increase in intense lake phytoplankton blooms since the 1980s. Nature 574 (7780), 667–670.

Huisman, J., Codd, G.A., Paerl, H.W., Ibelings, B.W., Verspagen, J.M.H., Visser, P.M., 2018. Cyanobacterial blooms. Nat. Rev. Microbiol. 16 (8), 471–483.

Jäger, C.G., Diehl, S., Schmidt, G.M., 2008. Influence of water-column depth and mixing on phytoplankton biomass, community composition, and nutrients. Limnol. Oceanogr. 53 (6), 2361–2373.

Janssen, A.B.G., Arhonditsis, G.B., Beusen, A., Bolding, K., Bruce, L., Bruggeman, J., Couture, R.M., Downing, A.S., Elliott, J.A., Frassl, M.A., Gal, G., Gerla, D.J., Hipsey, M.R., Hu, F.J., Ives, S.C., Janse, J.H., Jeppesen, E., Johnk, K.D., Kneis, D., Kong, X.Z., Kuiper, J.J., Lehmann, M.K., Lemmen, C., Ozkundakci, D., Petzoldt, T., Rinke, K., Robson, B.J., Sachse, R., Schep, S.A., Schmid, M., Scholten, H., Teurlincx, S., Trolle, D., Troost, T.A., Van Dam, A.A., Van Gerven, L.P.A., Weijerman, M., Wells, S.A., Mooij, W.M., 2015. Exploring, exploiting and evolving diversity of aquatic ecosystem models: a community perspective. Aquat. Ecol. 49 (4), 513–548.

Jeppesen, E., Jensen, J.P., Søndergaard, M., 2002. Response of phytoplankton, zooplankton, and fish to re-oligotrophication: an 11 year study of 23 Danish lakes. Aquat. Ecosys. Health Manag. 5 (1), 31–43.

Kalff, J., 2002. Limnology: Inland Water Ecosystems. Prentice Hall, Upper Saddle River, NJ.

Kiuru, P., Ojala, A., Mammarella, I., Heiskanen, J., Kamarainen, M., Vesala, T., Huttula, T., 2018. Effects of climate change on CO2 concentration and efflux in a humic boreal lake: a modeling study. Journal of Geophysical Research-Biogeosciences 123 (7), 2212–2233.

Klausmeier, C.A., Litchman, E., 2001. Algal games: the vertical distribution of phytoplankton in poorly mixed water columns. Limnol. Oceanogr. 46 (8), 1998–2007.

Kraemer, B.M., Chandra, S., Dell, A.I., Dix, M., Kuusisto, E., Livingstone, D.M., Schladow, S.G., Silow, E., Sitoki, L.M., Tamatamah, R., McIntyre, P.B., 2017. Global patterns in lake ecosystem responses to warming based on the temperature dependence of metabolism. Global Change Biol. 23 (5), 1881–1890.

Lee, N., Grunwald, U., Rosenlieb, E., Mirletz, H., Aznar, A., Spencer, R., Cox, S., 2020. Hybrid Floating Solar Photovoltaics-Hydropower Systems: Benefits and Global Assessment of Technical Potential, vol. 162. Renewable Energy, pp. 1415–1427.

Lenard, T., Wojciechowska, W., 2013. Phytoplankton diversity and biomass during winter with and without ice cover in the context of climate change. Pol. J. Ecol. 61 (4), 739–748.

Livingstone, D.M., Adrian, R., 2009. Modeling the duration of intermittent ice cover on a lake for climate-change studies. Limnol. Oceanogr. 54 (5), 1709–1722.

Longhi, M.L., Beisner, B.E., 2009. Environmental factors controlling the vertical distribution of phytoplankton in lakes. J. Plankton Res. 31 (10), 1195–1207.

Maltby, E., Ormerod, S., Acreman, M., Dunbar, M., Jenkins, A., Maberly, S., Newman, J., Blackwell, M., Ward, R., 2011. Freshwaters: Openwaters, Wetlands and Floodplains', *UK National Ecosystem Assessment: Understanding Nature's Value to Society*. UNEP-WCMC, Cambridge, UK, pp. 295–360.

Mantzouki, E., Visser, P.M., Bormans, M., Ibelings, B.W., 2016. Understanding the key ecological traits of cyanobacteria as a basis for their management and control in changing lakes. Aquat. Ecol. 50 (3), 333–350.

Markelov, I., Couture, R.M., Fischer, R., Haande, S., Van Cappellen, P., 2019. Coupling water column and sediment biogeochemical dynamics: modeling internal phosphorus loading, climate change responses, and mitigation measures in lake vansjo, Norway. Journal of Geophysical Research-Biogeosciences 124 (12), 3847–3866.

Met Office, 2019. MIDAS Open: UK Daily Weather Observation Data, v201908. Available at: https://catalogue.ceda.ac.uk/uuid/6ad6792f44c84c228651b01d182d9d73. Accessed: 16/02/21.

Meyer, K.M., Mooij, W.M., Vos, M., Hol, W.H.G., van der Putten, W.H., 2009. The power of simulating experiments. Ecol. Model. 220 (19), 2594–2597.

Moe, S.J., Haande, S., Couture, R.M., 2016. Climate change, cyanobacteria blooms and ecological status of lakes: a Bayesian network approach. Ecol. Model. 337, 330–347.

Momayez, M., Wilson, T., Cronin, A., Annavarapu, S., Conant, B.', 2009. An investigation to use tailing ponds as solar photovoltaic farms. 26th Annual Meetings of the American Society of Mining and Reclamation and 11th Billings Land Reclamation Symposium 817–832.

O'Neil, J.M., Davis, T.W., Burford, M.A., Gobler, C.J., 2012. The rise of harmful cyanobacteria blooms: the potential roles of eutrophication and climate change. Harmful Algae 14, 313–334.

Oliveira-Pinto, S., Stokkermans, J., 2020. 'Assessment of the Potential of Different Floating Solar Technologies - Overview and Analysis of Different Case Studies', Energy Conversion and Management, vol. 211, 112747.

Paerl, H.W., 2014. Mitigating harmful cyanobacterial blooms in a human- and climatically-impacted world. Life 4 (4), 988–1012.

Paerl, H.W., Havens, K.E., Hall, N.S., Otten, T.G., Zhu, M., Xu, H., Zhu, G., Qin, B., 2019. Mitigating a global expansion of toxic cyanobacterial blooms: confounding effects and challenges posed by climate change. Mar. Freshw. Res. 71 (5), 579–592.

Page, T., Smith, P.J., Beven, K.J., Jones, I.D., Elliott, J.A., Maberly, S.C., Mackay, E.B., De Ville, M., Feuchtmayr, H., 2018. Adaptive forecasting of phytoplankton communities. Water Res. 134, 74–85.

Pilla, R.M., Couture, R.M., 2021. Attenuation of photosynthetically active radiation and ultraviolet radiation in response to changing dissolved organic carbon in browning lakes: modeling and parametrization. Limnol. Oceanogr. 66 (6), 2278–2289.

Plaas, H.E., Paerl, H.W., 2021. Toxic cyanobacteria: a growing threat to water and air quality. Environ. Sci. Technol. 55 (1), 44–64.

Reynaud, A., Lanzanova, D., 2017. A global meta-analysis of the value of ecosystem services provided by lakes. Ecol. Econ. 137, 184–194.

Reynolds, C., Irish, T., Elliott, A., 2005. A modelling approach to the development of an active management strategy for the Queen Elizabeth II reservoir. Freshw. Forum 23 (1).

Reynolds, C.S., 1997. Vegetation Processes in the Pelagic: a Model for Ecosystem Theory. Ecology Institute Oldendorf, Luhe, Hamburg.

Reynolds, C.S., 2006. The ecology of phytoplankton. In: Ecology, Biodiversity and Conservation. Cambridge University Press, Cambridge.

Reynolds, C.S., Huszar, V., Kruk, C., Naselli-Flores, L., Melo, S., 2002. Towards a functional classification of the freshwater phytoplankton. J. Plankton Res. 24 (5), 417–428.

Reynolds, C.S., Irish, A.E., Elliott, J.A., 2001. The ecological basis for simulating phytoplankton responses to environmental change (PROTECH). Ecol. Model. 140 (3), 271–291.

Reynolds, C.S., Oliver, R.L., Walsby, A.E., 1987. Cyanobacterial dominance: the role of buoyancy regulation in dynamic lake environments. N. Z. J. Mar. Freshw. Res. 21 (3), 379–390.

Ross, O.N., Sharples, J., 2008. Swimming for survival: a role of phytoplankton motility in a stratified turbulent environment. J. Mar. Syst. 70 (3–4), 248–262.

Sacramento, E.M.d., Carvalho, P.C.M., de Araújo, J.C., Riffel, D.B., Corrêa, R.M.d.C., Pinheiro Neto, J.S., 2015. Scenarios for use of floating photovoltaic plants in Brazilian reservoirs. IET Renew. Power Gener. 9 (8), 1019–1024.

Sahu, A., Yadav, N., Sudhakar, K., 2016. Floating Photovoltaic Power Plant: A Review, vol. 66. Renewable & Sustainable Energy Reviews, pp. 815–824.

Salk, K.R., Venkiteswaran, J.J., Couture, R.M., Higgins, S.N., Paterson, M.J., Schiff, S.L., 2022. Warming combined with experimental eutrophication intensifies lake phytoplankton blooms. Limnol. Oceanogr. 67 (1), 147–158.

Salmaso, N., Naselli-Flores, L., Padisak, J., 2015. Functional classifications and their application in phytoplankton ecology. Freshw. Biol. 60 (4), 603–619.

Saloranta, T., Andersen, T., 2004. MyLake v1.1: technical documentation & user's guide: Norwegian Institute for Water Research (NIVA report 4838. Available at: https://niva.brage.unit.no/niva-xmlui/bitstream/handle/11250/212445/4838_200dpi.pdf?sequence=2&isAllowed=y.

Saloranta, T.M., Andersen, T., 2007. MyLake - a multi-year lake simulation model code suitable for uncertainty and sensitivity analysis simulations. Ecol. Model. 207 (1), 45–60.

Sanchez, R.G., Kougias, I., Moner-Girona, M., Fahl, F., Jäger-Waldau, A., 2021. Assessment of Floating Solar Photovoltaics Potential in Existing Hydropower Reservoirs in Africa, vol. 169. Renewable Energy, pp. 687–699.

Shimoda, Y., Arhonditsis, G.B., 2016. Phytoplankton functional type modelling: running before we can walk? A critical evaluation of the current state of knowledge. Ecol. Model. 320, 29–43.

Spencer, R.S., Macknick, J., Aznar, A., Warren, A., Reese, M.O., 2019. Floating photovoltaic systems: assessing the technical potential of photovoltaic systems on man-made water bodies in the continental United States. Environ. Sci. Technol. 53 (3), 1680–1689.

Stewart-Oaten, A., Murdoch, W.W., Parker, K.R., 1986. Environmental impact assessment:" Pseudoreplication" in time? Ecology 67 (4), 929–940.

Stiubiener, U., da Silva, T.C., Trigoso, F.B.M., Benedito, R.D., Teixeira, J.C., 2020. PV power generation on hydro dam's reservoirs in Brazil: a way to improve operational flexibility. Renew. Energy 150, 765–776.

Ta, T., 2019. Queen Elizabeth II (QEII) Reservoir Computational Fluid Dynamics (CFD) Model for Cryptosporidium Residence Time (Unpublished report prepared for Thames Water).

Umlauf, L., Burchard, H., Bolding, K., 2005. GOTM Sourcecode and Test Case Documentation. Devel version-pre, p. 4.

Visser, P.M., Ibelings, B.W., Bormans, M., Huisman, J., 2015. Artificial mixing to control cyanobacterial blooms: a review. Aquat. Ecol. 50 (3), 423–441.

Woolway, R.I., Meinson, P., Noges, P., Jones, I.D., Laas, A., 2017. Atmospheric stilling leads to prolonged thermal stratification in a large shallow polymictic lake. Climatic Change 141 (4), 759–773.

Wright, R.T., 1964. Dynamics of a phytoplankton community in an ice-covered lake. Limnol. Oceanogr. 9 (2), 163–178.

Yadav, N., Gupta, M., Sudhakar, K., 2016. Energy assessment of floating photovoltaic system. International Conference on Electrical Power and Energy Systems 264–269. https://doi.org/10.1109/ICEPES.2016.7915941, 2016.

Yamamichi, M., Kazama, T., Tokita, K., Katano, I., Doi, H., Yoshida, T., Hairston Jr., N.G., Urabe, J., 2018. A shady phytoplankton paradox: when phytoplankton increases under low light. Proc. Biol. Sci. 285, 20181067, 1882.

Zhang, N., Jiang, T., Guo, C., Qiao, L.F., Ji, Q., Yin, L.Q., Yu, L.M., Murto, P., Xu, X.F., 2020. High-performance semitransparent polymer solar cells floating on water: rational analysis of power generation, water evaporation and algal growth. Nano Energy 77, 105111.

Zhang, W.T., Rao, Y.R., 2012. Application of a eutrophication model for assessing water quality in Lake Winnipeg. J. Great Lake. Res. 38, 158–173.

Ziar, H., Prudon, B., Lin, F.Y., Roeffen, B., Heijkoop, D., Stark, T., Teurlincx, S., Domis, L. D., Goma, E.G., Extebarria, J.G., Alavez, I.N., van Tilborg, D., van Laar, H., Santbergen, R., Isabella, O., 2021. Innovative floating bifacial photovoltaic solutions for inland water areas. Progress in Photovoltaics 29 (7), 725–743.